

# Adsorption of carbon dioxide of 1-site and 3-site models in pillared clays: A Gibbs ensemble Monte Carlo simulation

Xuan Peng<sup>a</sup>, Jinsong Zhao<sup>a</sup>, Dapeng Cao<sup>b,\*</sup>

<sup>a</sup> *Laboratory for Intelligent Process Systems Engineering, College of Information Science and Technology, Beijing University of Chemical Technology, Beijing 100029, PR China*

<sup>b</sup> *Division of Molecular and Materials Simulation, Key Laboratory of Nanomaterials, Ministry of Education, Beijing University of Chemical Technology, Beijing 100029, PR China*

Received 9 October 2006; accepted 3 February 2007

Available online 12 February 2007

## Abstract

Adsorption behavior of carbon dioxide confined in pillared clays is analyzed by using constant pressure Gibbs ensemble Monte Carlo (GEMC) method. In our simulation, 1-site and 3-site models are used to represent carbon dioxide. At the 1-site model, carbon dioxide is described as a Lennard–Jones (LJ) sphere, while at the 3-site model, carbon dioxide is modeled as a three-sites linear chain represented by EPM2 potential considering the quadrupolar effect. The potential model from Yi et al. for pillared clays is used to emphasize its quasi two-dimensional structure. Comparing the calculated results from the 1-site and the 3-site models at  $T = 228.15$  and  $258.15$  K, we observe that the adsorption amount from the two models is the same basically. However, the local density presents a significant difference, because the shoulder in the main peak near the wall from 3-site model can reflect the orientation of carbon dioxide. Accordingly, in the systematical investigation to explore the effect of porosity and pore width on the adsorption of carbon dioxide in pillared clays, the 3-site model was only used. We observe that for a narrow pore of  $H = 1.02$  nm, each isotherm shape displays type I curve, suggesting that it is not inflected by the porosity. However, for the larger pores of  $H = 1.70$  and  $H = 2.38$  nm, the increase of the porosity alters the shape of adsorption isotherms from a simple linear relation to the first order jump, indicating that the porosity is of very important factor to affect adsorption and phase behavior of fluids confined in pillared clays. The excess adsorptions of carbon dioxide at supercritical temperatures of  $T = 323.15$  and  $348.15$  K are also investigated. We find that the maximum exists for each excess isotherm, and the optimal pressure corresponding to the maximum increases with the pore width. However, the porosity has no significant effect on the optimal pressure.

© 2007 Elsevier Inc. All rights reserved.

**Keywords:** Adsorption; Carbon dioxide; Pillared clay; Gibbs ensemble Monte Carlo simulation

## 1. Introduction

The increasing concentration of carbon dioxide in atmosphere, mainly caused by fossil fuel combustion, has led to concerns about global warming. Capture and disposal of carbon dioxide are thus considered as an efficient means to avoid this problem. Furthermore, in the presence of water, carbon dioxide would corrupt the vessels and cylinders for the transportation and storage of natural gas. Therefore, removing carbon dioxide to effectively utilize natural gas becomes an important subject.

Currently, one way that can contribute to the sequestration of carbon dioxide is removing it from the atmosphere by pumping into a huge aquifer beneath the ocean floor or into soils underground [1,2]. Another issue involves the removal of greenhouse gases directly from industrial plant exhaust and subsequently storing them in secure reservoirs [2]. In the first case, the soils usually contain abundant clay minerals, which mainly contain montmorillonite. The natural montmorillonite is a sheet structure made up of a layer of octahedral aluminum oxide between two layers of tetrahedral silicon oxides. The spaces between sheets give rise to nanopores called the interlayer porosity, and the interparticle and interaggregate spaces form micro- and mesopores [3]. In the second case, adsorption technique using porous materials is still a prospective candidate for gas stor-

\* Corresponding author.

E-mail address: [caodp@mail.buct.edu.cn](mailto:caodp@mail.buct.edu.cn) (D. Cao).

age and other industrial processes, because of its high energy efficiency, low operating cost, and ease of control over a relatively wide range of pressures and temperatures [4]. Pillared clays (PILCs), as a class of porous material similar to zeolite-based catalysts, has caused a special concern for researchers in chemical engineering field. Although the PILCs were found in 1955 [5], interest on clays as catalysts was raised in the 1970s [6] with the development of pillared clays. Further details on history of discovery and application of those materials can be found elsewhere [7–9]. The most advantage of the PILCs material, similar to montmorillonite, is that the available interior pore volume can be tailored for some special applications during the preparation process by the distance between the opposite solid walls as well as the distribution of pillars [10]. Therefore, the PILCs are still very interesting and promising adsorbents. As a result, the PILCs materials are widely used in strategic industrial and environmental applications such as gas storage, shape selective catalysis, and separation.

Some extensive studies on adsorption of gases in the PILCs have been performed experimentally. In 1992, Baksh and Yang [11] measured the adsorption isotherms of O<sub>2</sub>, N<sub>2</sub>, CH<sub>4</sub>, CO<sub>2</sub>, SO<sub>2</sub>, and NO on five pillared clays (Zr, Al, Cr, Fe, and Ti-PILCs) and found the adsorption selectivity of CH<sub>4</sub>/N<sub>2</sub> on Al-PILC is greater than 5.0. In a subsequent work by Molinard and Vansant [12], the effects of cation modification on porosity and interlayer distance during sample preparation were investigated by adsorption isotherms of nitrogen at 77 K and XRD data. Moreover, their experiments of gases adsorption such as N<sub>2</sub>, O<sub>2</sub>, Ar or CO<sub>2</sub> in these different PILCs demonstrate that the adsorption properties of these PILCs depend mainly on the pillar height, the distribution of the pillars between the clay layers, and the nature of the pillaring species. In 1998, Pereira et al. [13] investigated the adsorption of CH<sub>4</sub> and CO<sub>2</sub> on zirconium oxide intercalated clays by both experiment and vacancy solution theory. Recently, Gil and Ganda [14] employed the Dubinin–Astakhov (DA) equation, the Horvath–Kawazoe (HK), the Jaroniec–Gadkaree–Choma (JGC) methods, and the density functional theory (DFT) to characterize the microporous structure of an alumina intercalated clay from adsorption of nitrogen and carbon dioxide. They found that high calcination temperatures would significantly deteriorate the ultramicropores rather than mesopores during pillaring process.

Alternatively, computer simulation provides a versatile and powerful means to investigate the adsorption of confined fluids in this type of materials. In 1995, Yi et al. [15] studied the thermodynamics and transport properties of Lennard–Jones (LJ) fluids in pillared clays by a molecular dynamics (MD) method. In a subsequent paper [16], they reported the adsorption of single component and binary gas mixtures confined in layered pillared pores. In 2000, Ghassemzadeh et al. [17] addressed the separation of three binary mixtures confined in layered pillared pores and molecular sieve membranes at temperature  $T = 303$  K, using the equilibrium MD method. Later, Cao and Wang reported the phase behavior of methane confined in layered pillared pores at low temperatures [18], and recommended the layered pillared pore material with porosity of 0.94 and pore width of 1.02 nm as the optimum adsorption

storage materials for supercritical methane [19]. In addition, adsorption recovery of CCl<sub>4</sub> in pillared clays was compared to that in activated carbon by grand canonical Monte Carlo (GCMC) simulation [20], which reveals that the former gives higher uptake and the capillary condensation transition takes place at lower pressure. More recently, the adsorption and microstructure of HCFC-22 in pillared clays by the combination of GCMC simulations and quantum mechanics calculations are reported [21]. Peng et al. [22] simulated the chemical equilibrium of ammonia synthesis in pillared clays and obtained the higher ammonia mole fraction than in slit pores due to the greater uptake. For the adsorption of carbon dioxide on other materials, Zhou and Wang [23] simulated the adsorption and diffusion of carbon dioxide confined in slit pores from sub- to super-critical conditions using a combination of GCMC and MD methods. The adsorption of pure-component and binary mixtures of methane and carbon dioxide in a specific activated carbon was predicted using GCMC and pore size distribution (PSD) method [24]. Sweatman and Quirke [25] employed a combination of GCMC and Gibbs Monte Carlo simulations to characterize amorphous materials and believed that adsorption isotherms of carbon dioxide at room temperature could provide more accurate description of carbon microstructure than traditional nitrogen isotherms at 77 K. Peng and Wang [4] carried out experimental and theoretical studies for the removal of carbon dioxide from the mixture of CH<sub>4</sub>/CO<sub>2</sub> by the activated Mesocarbon Microbead adsorbent.

The investigation results from Molinard and Vansant [12] reveals that a simple model from Yi et al. [15] can basically meet the requirement of computer simulation, because it contains two important characteristics of this material, namely, pore width (i.e., the pillar height), and porosity (i.e., the distribution of the pillars between the clay layers). Therefore, the purpose of this work is to explore the effects of pore width and porosity, as well as temperature and pressure, on the adsorption isotherms of carbon dioxide in pillared clays, by using molecular simulation tool. This information would definitely provide a deep insight into materials and process design, development and optimization.

## 2. Molecular models of pillared clays

The diffusion of the simple LJ fluid confined in layered pillared pores had been studied by Yi et al. using MD method [15]. Their results indicate that different distributions of the pillar had very little effect on the adsorption. Therefore, an ideal model [15] with uniform distribution of pillars between two layered walls is directly adopted to describe the pillared clays. Although this model is relatively crude, it provides a simple idealized model that incorporates the important physical characteristics for this study. A schematic diagram of the material is shown in Fig. 1, where two layered solid walls are represented by the surfaces with the specified surface number density, and the pillars are represented by rigid chains consisting of a given number of carbon atoms with the size parameter  $\sigma_p$ . Defining the perpendicular direction of the layered solid walls as the  $z$ -direction, the coordinate of the center of the end molecules in the pillar

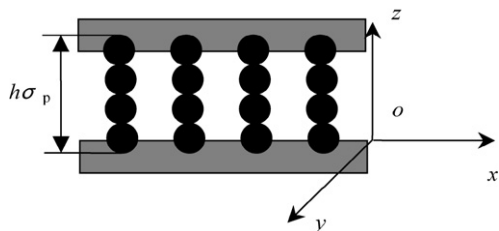


Fig. 1. Schematic representation (side view) of the model of pillared clays with pore width  $H = h\sigma_p$ , where  $h$  is the number of atoms composing one pillar,  $\sigma_p$  is the pillar atom size.

Table 1  
Potential parameters of carbon dioxide, pillar and solid wall

Fluid and pore	Atom	$bl$ (nm)	$q$ (e)	$\sigma$ (nm)	$(\varepsilon/k_b)$ (K)
CO <sub>2</sub> (3-site)	C	0.0	0.6512	0.2757	28.129
	O	0.1149	-0.3256	0.3033	80.507
CO <sub>2</sub> (1-site)	–	–	–	0.375	236.1
Pillar	C	0.0	0.0	0.34	28.0
Solid wall	C	0.0	0.0	0.34	28.0

Note.  $bl$  is the distance from the interaction site to molecular mass center. The 3-site EPM2 model [26] is used to describe carbon dioxide molecule, and compared with the 1-site model from literature [30]. The potential of C atom is used to denote pillar and solid wall.

chain is zero. The distance (i.e., the pore width) between two layered solid walls is defined as the pillar height  $h\sigma_p$ , where  $h$  is the number of pillar atoms. The porosity  $\psi$  is defined as the volume fraction of the porous material not occupied by the pillars,

$$\psi = 1 - \frac{N_p \pi \sigma_p^2}{6S}, \quad (1)$$

where  $N_p$  is the number of pillars and  $S$  is the area in the  $x$ – $y$  surface in the simulation box.

For a fluid molecule confined in pillared clays, its total potential energy is a sum of three interactions: the potential energy between fluid molecules,  $\phi_{ff}$ , the potential energy between a fluid molecule and a layered wall,  $\phi_{fw}$ , and the potential energy between a fluid molecule and pillars,  $\phi_{fp}$ . All the model parameters are listed in Table 1, and their cross energy and size parameters are calculated by Lorentz–Berthelot (LB) mixing rule.

### 2.1. Fluid–fluid interaction

For the 3-site model taking into account of quadrupolar effect, the linear carbon dioxide molecule is described by effective EPM2 potential [26] as a three-center LJ plus a set of partial point charges distributed at three electrostatic sites. Thus, the fluid–fluid interaction  $\phi_{ff}$  is composed of the LJ potential and electrostatic interaction of sites  $m$  on molecule  $i$  with the site  $n$  on molecule  $j$ ,

$$\phi_{ff} = 4 \sum_{im} \sum_{jn} \varepsilon_{im,jn} \left[ \left( \frac{\sigma_{im,jn}}{r_{im,jn}} \right)^{12} - \left( \frac{\sigma_{im,jn}}{r_{im,jn}} \right)^6 \right] + \sum_{im} \sum_{jn} \frac{q_{im} q_{jn}}{r_{im,jn}}, \quad (2)$$

where the subscripts  $i$  and  $j$  denote different molecular species;  $m$  and  $n$  are the sites on the molecules  $i$  and  $j$ , respectively.  $\varepsilon$  and  $\sigma$  are the energy and size parameters of site–site from the LB combining rule,  $q$  is the charge of different sites,  $r_{im,jn}$  is the inter-site distance.

The 1-site model describes carbon dioxide only as one spherical particle. Therefore, the quadrupolar effect is not considered. The fluid–fluid interaction is represented only by the LJ potential, given by

$$\phi_{ff} = 4\varepsilon_{ff} \left[ \left( \frac{\sigma_{ff}}{r_{ij}} \right)^{12} - \left( \frac{\sigma_{ff}}{r_{ij}} \right)^6 \right]. \quad (3)$$

The potential parameters [23] of carbon dioxide for the 1-site model are also given in Table 1.

### 2.2. Fluid–wall interaction

The interaction between a fluid molecule and a solid wall is given by the well-known Steele’s 10–4–3 potential [27], where only an independent variable of the normal distance between a fluid molecule and one of the solid walls,  $z$ , is included,

$$\phi_{fw}(z) = 2\pi\rho_w\varepsilon_{fw}\sigma_{fw}^2\Delta \left[ 0.4 \left( \frac{\sigma_{fw}}{z} \right)^{10} - \left( \frac{\sigma_{fw}}{z} \right)^4 - \left( \frac{\sigma_{fw}^4}{3\Delta(0.61\Delta + z)^3} \right) \right], \quad (4)$$

where  $\sigma_{fw}$  and  $\varepsilon_{fw}$  are cross fluid–wall interaction parameters.  $\rho_w$  is the number density of carbon atoms on the solid wall,  $\rho_w = 114.0 \text{ nm}^{-3}$ , and  $\Delta$  is the distance between lattice planes,  $\Delta = 0.335 \text{ nm}$ .

### 2.3. Fluid–pillar interaction

The potential between a fluid molecule and the pillar atoms,  $\phi_{fp}$ , is generally described by the site-to-site method [20],

$$\phi_{fp} = 4\varepsilon_{fp} \sum_{i=1}^{hN_p} \sum_{j=1}^{N_f} \left[ \left( \frac{\sigma_{fp}}{r_{ij}} \right)^{12} - \left( \frac{\sigma_{fp}}{r_{ij}} \right)^6 \right], \quad (5)$$

where  $r_{ij}$  is the distance between a site of fluid molecules and an atom of pillars,  $N_f$  is the number of fluid molecules in the simulation box,  $\varepsilon_{fp}$  and  $\sigma_{fp}$  are the cross interaction parameters.

## 3. Simulation details

Adsorption isotherms are generally described as a function of the pressure of the bulk fluid. When a grand canonical Monte Carlo (GCMC) simulation is performed, the chemical potential can be generally converted to the pressure either through an accurate equation of state (EOS) for fluids or by Widom particle inserting method during the simulation process. In this work, an alternative approach to avoid the conversion from chemical potential to pressure in GCMC, is to use the constant pressure Gibbs ensemble Monte Carlo (GEMC) method [28,29] to simulate the adsorption behavior of carbon dioxide in pillared clays.

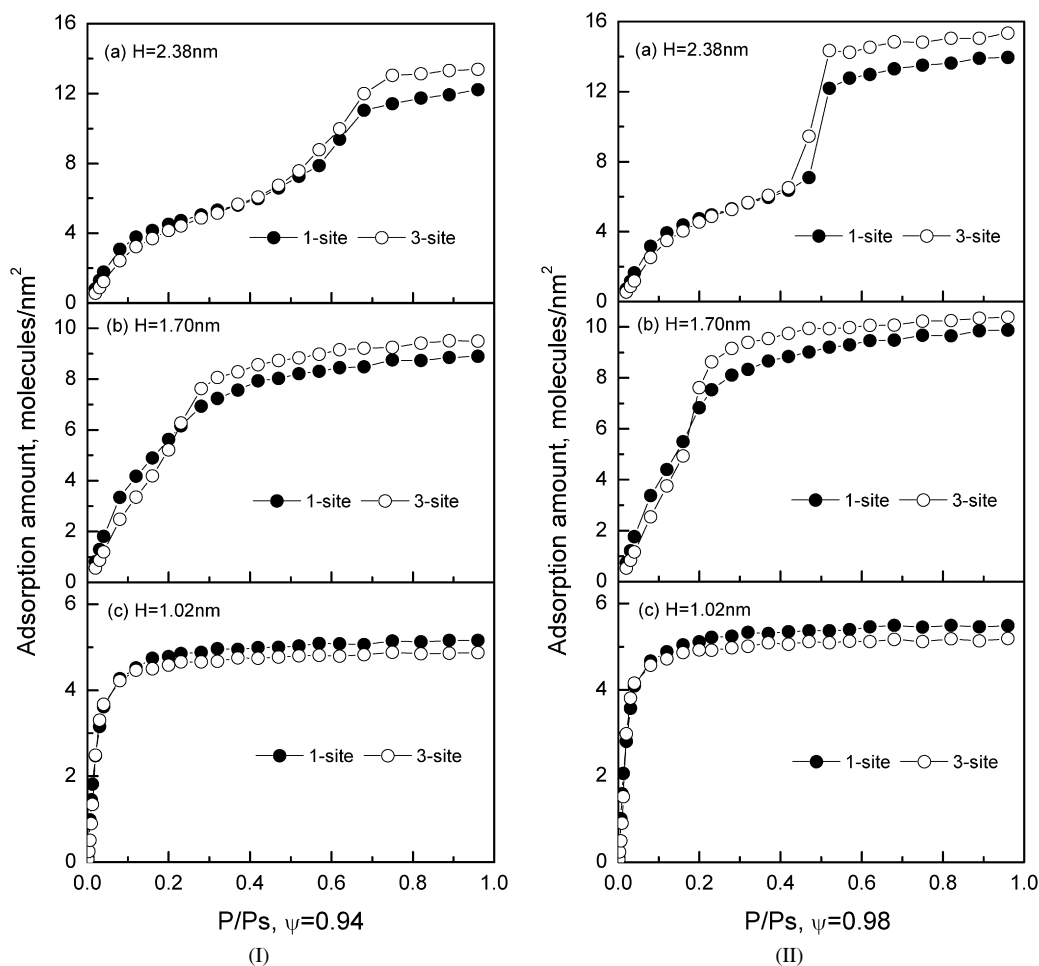


Fig. 2. Comparison of adsorption isotherms of carbon dioxide by 1-site and 3-site models at 228.15 K, where solid and open circles denote 1-site and 3-site, respectively.

One of the most attracting advantages of this technique is that it uses the pressure of bulk phase as an input parameter to avoid the specification of chemical potential or fugacity in GCMC method. In the GCMC method, two simulation cells, which one represents the pore phase and the other for the coexisting bulk phase, are performed simultaneously. For the pore phase, the two walls are fixed on top and bottom sides of the simulation box, and pillars are uniformly distributed between two walls. The total number of particles  $N$  in both cells, the volume of the pore  $V_p$  and the temperature  $T$  are fixed in the simulation. A GCMC procedure contains three types of move, that is, particle displacement (including translation and rotation) in both cells with the usual Metropolis scheme, particle exchange to ensure the chemical potential equilibrium between bulk and pore phases, and the random perturbation in the volume of the bulk cell to ensure the bulk pressure fixed.

In the simulation, the periodic boundary condition is imposed on the  $x$ - $y$  plane perpendicular to the  $z$ -direction for the pore phase. Before the start of simulations, we generated about four thousands of carbon dioxide molecules in the bulk phase. With the process of the simulation, the molecules gradually enter the pore phase under the criteria of the GCMC. The cut-off radius is set to 3.32 nm for the LJ and electrostatic potentials. To

ensure the electrostatic contribution beyond this cutoff less than 1% of the total energy, Ewald summation technique is used. For each state point, the first  $1 \times 10^7$  GCMC moves are discarded to guarantee the equilibrium, and the followed  $1 \times 10^7$  GCMC moves are adopted for ensemble average of the desired thermodynamic properties. The acceptance criteria of three trial moves are depicted elsewhere [28,29].

## 4. Results and discussion

### 4.1. Comparison of adsorption of carbon dioxide in pillared clays by 3-site and 1-site models

As we known, a real carbon dioxide molecule is composed of 1 oxygen and 2 carbon atoms, 3-site potential model proposed by Harris [26] considers the orientation of carbon dioxide, and can naturally describe its physical characteristics. However, some researchers [23,30] also used a spherical Lennard–Jones particle to represent carbon dioxide for less computational time. Vishnyakov et al. [31] made a comprehensive comparison between 1-site and 3-site models, in particular. Their results reveal that the two models give excellent agreement for adsorption isotherms of carbon dioxide in slit pores, though an entirely different density profiles for the confined

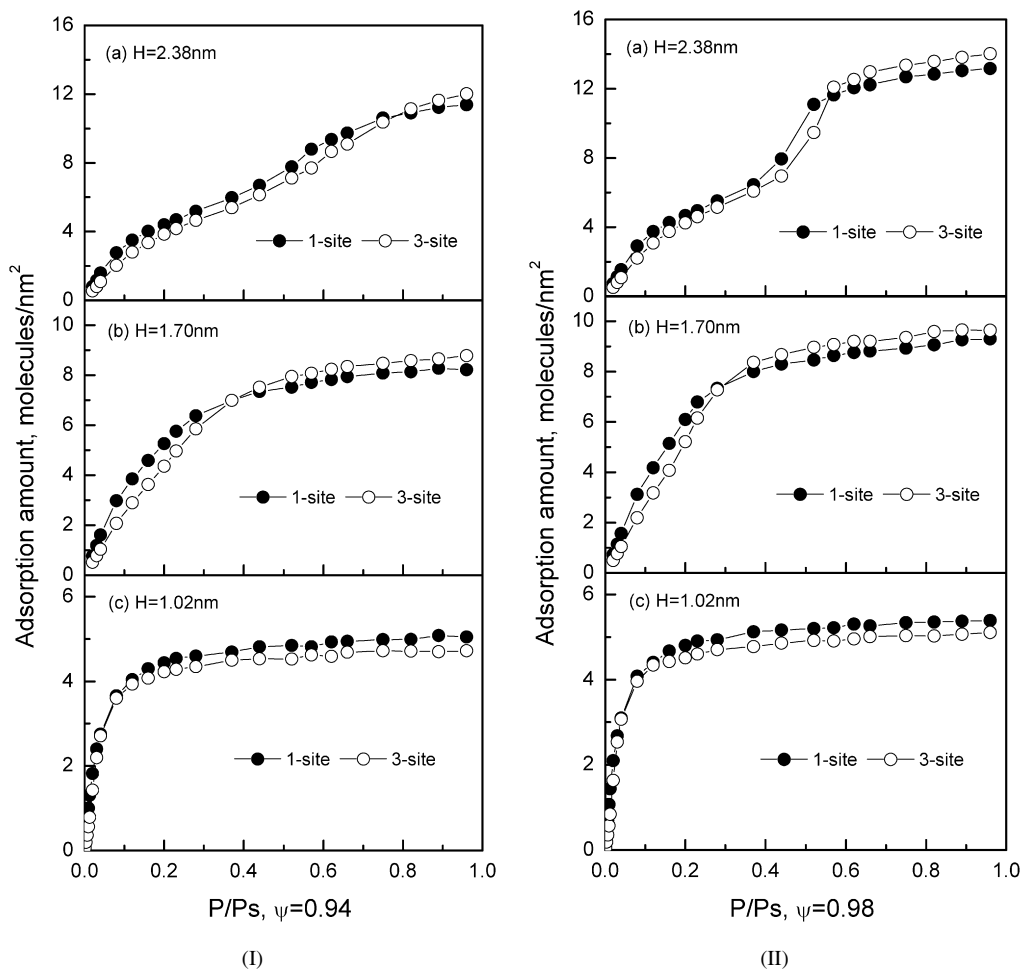


Fig. 3. Comparison of adsorption isotherms of carbon dioxide by 1-site and 3-site models at 258.15 K, where solid and open circles denote 1-site and 3-site, respectively.

carbon dioxide is observed. Analogously, Do and Do [32] evaluated the performance of three intermolecular potential models (TraPPE, HMT and 5-Charge) on the adsorption of carbon dioxide on graphitized thermal carbon black at various temperatures and in carbon slits. They found that the adsorption isotherms are well described by the TraPPE model, while the isosteric heat is only reasonably described. In addition, the HMT under-predicts the data while the 5-Charge model over-predicts it. Therefore, here we intend to explore the performance of the 1-site and 3-site models for the adsorption of carbon dioxide in pillared clays.

Figs. 2 and 3 show the comparison of adsorption isotherms of carbon dioxide at  $T = 228.15$  and  $258.15$  K by 1-site and 3-site models, respectively. For all pore widths and porosities studied, the adsorption isotherms for both models are in consistent agreement except that at high pressure, the adsorption amount has a slight difference. For the larger pore of  $H = 2.38$  nm, even the positions corresponding to the adsorption jump are also the same, as shown in Fig. 2a. The slight difference at high pressure is due to the shape of the molecule. At the small pore of  $H = 1.02$  nm, the spherical geometry is the easier for the packing of molecules in pores than the linear chain geometry. Therefore, the adsorption amount from the

1-site model is slightly larger than that from the 3-site model at the high pressure. However, at the larger pore of  $H = 1.7$  and  $2.38$  nm, the linear chain is easier for the packing of molecules in pores than the spherical molecule, because the diameter of the spherical molecule is around 1.3 times of that of the site from the 3-site model. Accordingly, in this case, the adsorption amount from the 3-site model is slightly larger than that from 1-site model at the high pressure. In summary, the two models have no significant effect on adsorption and isotherm shape of carbon dioxide in pillared clays. Although the quadrupolar effect has taken into account in the 3-site model, the polar group was not introduced into the pillared clays materials. Accordingly, the quadrupolar moment presented in the 3-site model did not show significant effect on the adsorption of carbon dioxide, leading to that the adsorption isotherms from the two models are the same basically. In our future work, the COOH polar group would be introduced into the pillared clays in order to investigate the effect of functional groups on adsorption isotherms of carbon dioxide.

To provide further insights into the difference between the 1-site and 3-site models, we also present in Fig. 4 the local density profiles at  $\psi = 0.94$ ,  $H = 2.38$  nm, and  $T = 228.15$  and  $258.15$  K, respectively. Interestingly, the local density from the

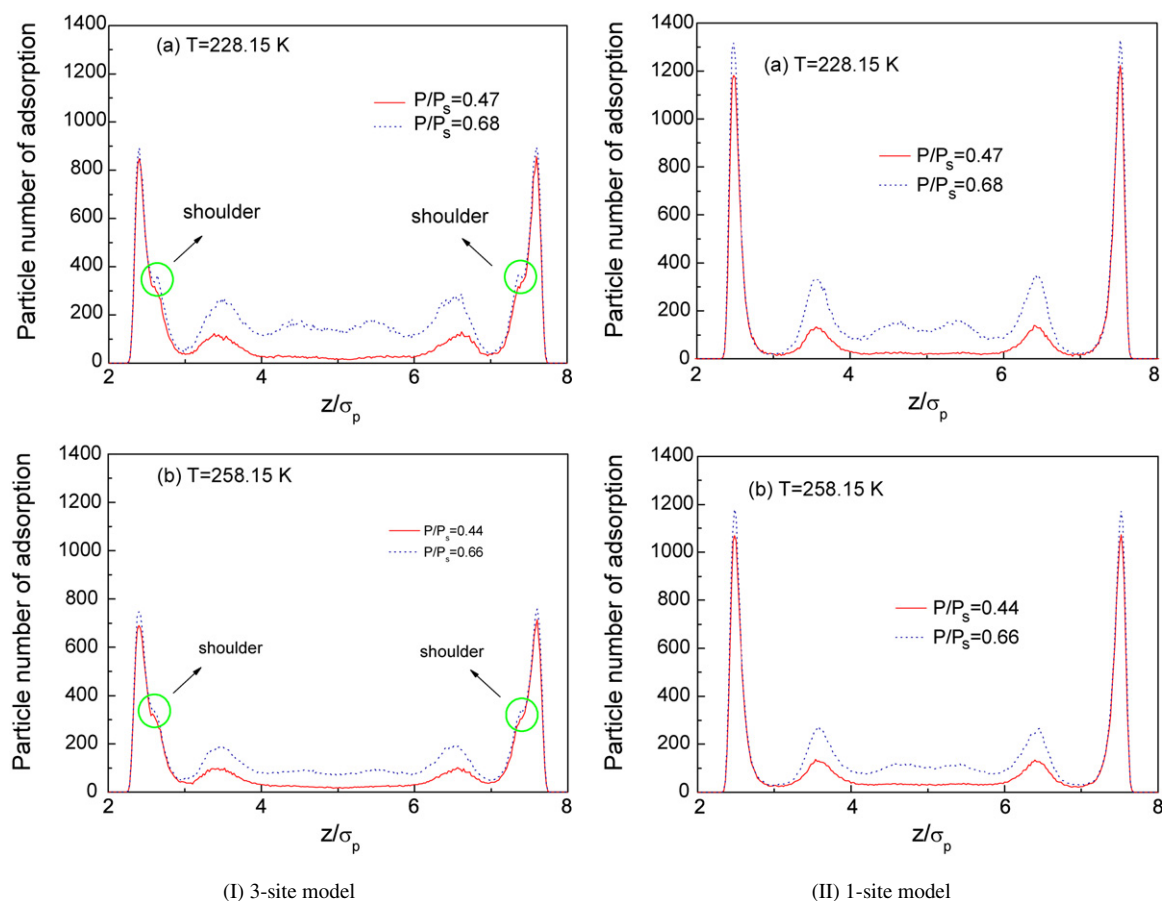


Fig. 4. Local density profile of mass center of carbon dioxide in pillared clays by 3-site and 1-site models at  $\psi = 0.94$  and  $H = 2.38$  nm. (I) The 3-site model, (II) the 1-site model; (a)  $T = 228.15$  K, where line is for  $P/P_s = 0.47$  and point is for  $P/P_s = 0.68$ , (b)  $T = 258.15$  K, where line is for  $P/P_s = 0.44$  and point is for  $P/P_s = 0.66$ .

3-site model presents a main peak and a shoulder (highlighted by green circle) near the wall, while the local density from the 1-site model only presents a major peak without any shoulder near the wall. The presence of the shoulder for the 3-site model is because the orientation of the 3-site molecule is not parallel to the wall. For the 1-site model, the molecule has no any orientations. Accordingly, the local density only presents one peak near the wall. To illustrate further, four snapshots for the two models at 228.15 K and two different pressures are presented in Figs. 5 and 6, respectively. Compared to Fig. 6, carbon dioxide molecules in Fig. 5 show distinct spatial orientation. In particular, we use green circle to highlight the molecules lean against the wall, as shown in Fig. 5, I-(b). It is the spatial orientation of molecules that causes the shoulder of local density profiles presented in Fig. 4.

#### 4.2. Phase behavior of carbon dioxide confined in pillared clays at low temperatures

By comparing the 1-site and 3-site models, we find that the two models have no significant effect on adsorption behavior of carbon dioxide, while the local density profiles present some difference due to the molecular shapes. Obviously, the 3-site model can more accurately represent the microscopic and macroscopic properties, because the shape and quadrupole

of carbon dioxide can be reflected in the model. Accordingly, we only use the 3-site model in the following sections for its more elaborated representation of the real molecule. To give insight into the phase behavior of carbon dioxide confined in pillared clays, we simulated the systems with three porosities,  $\psi = 0.88, 0.94$  and  $0.98$  and three different pore widths,  $H = 1.02, 1.70$  and  $2.38$  nm at low temperatures,  $T = 228.15$  and  $258.15$  K. The calculated results were shown in Fig. 7.

It can be observed from Fig. 7 that at  $T = 258.15$  K, the adsorption amount of carbon dioxide is less than that at  $T = 228.15$  K, it is because with the enhancement of molecular kinetic energy, the interaction is weakened between fluids and pore walls. In addition, we also found that at the narrow pore of  $H = 1.02$  nm, all adsorption isotherms present the Langmuir type, i.e. type-I [33] isotherm in micropores. However, at the larger pore of  $H = 1.70$  and  $H = 2.38$  nm, the shape of the isotherm shows the complicated behavior of non-Langmuir type. For example, at the smaller porosity of  $\psi = 0.88$ , the adsorption isotherm shape is almost linear increase with pressure at two temperatures. Whereas at the porosities of  $\psi = 0.94$  and  $0.98$ , the rising of isotherms becomes more steep at lower  $T = 228.15$  K. More interestingly, at  $\psi = 0.94$  and  $H = 2.38$  nm, a clear S-shaped isotherm is observed at  $T = 228.15$  K (see Fig. 7, I-(a)), corresponding to the adsorption isotherm of type IV [33] in mesopores, but it only shows

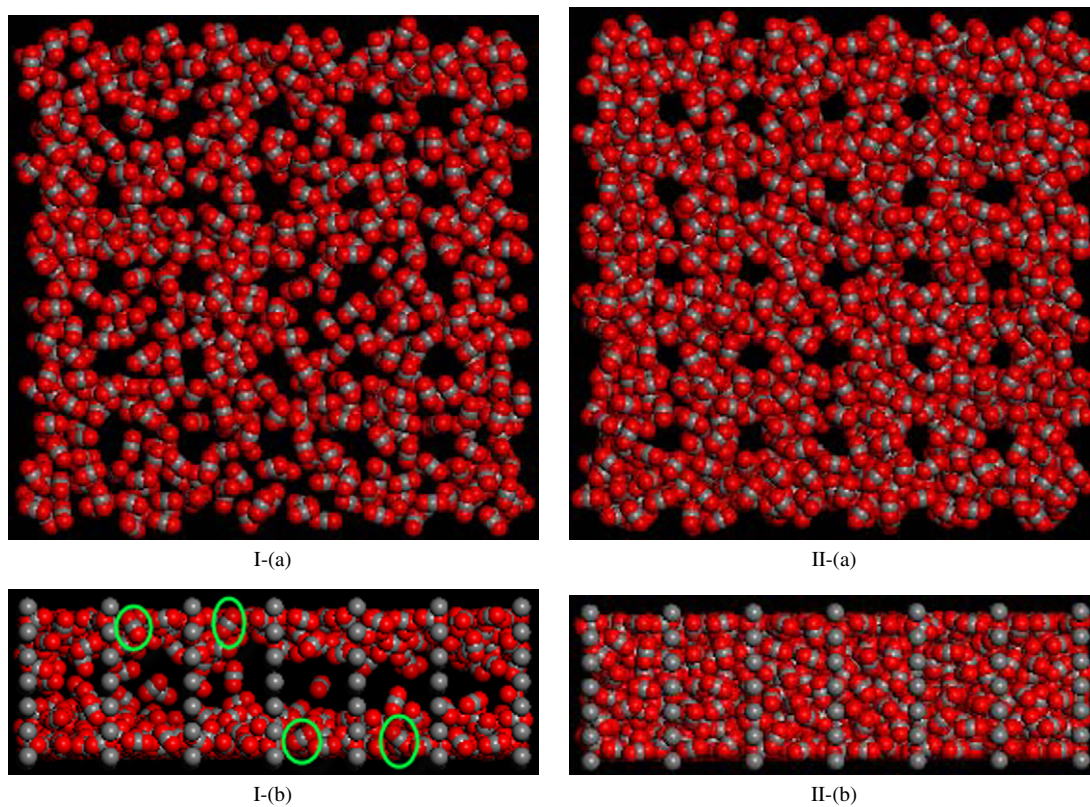


Fig. 5. Snapshots of carbon dioxide confined in pillared clays by the 3-site model at  $T = 228.15$  K,  $\psi = 0.94$ , and  $H = 2.38$  nm. (I)  $P/P_s = 0.47$ , (II)  $P/P_s = 0.68$ ; (a) from  $z$ -axis, (b) from  $y$ -axis.

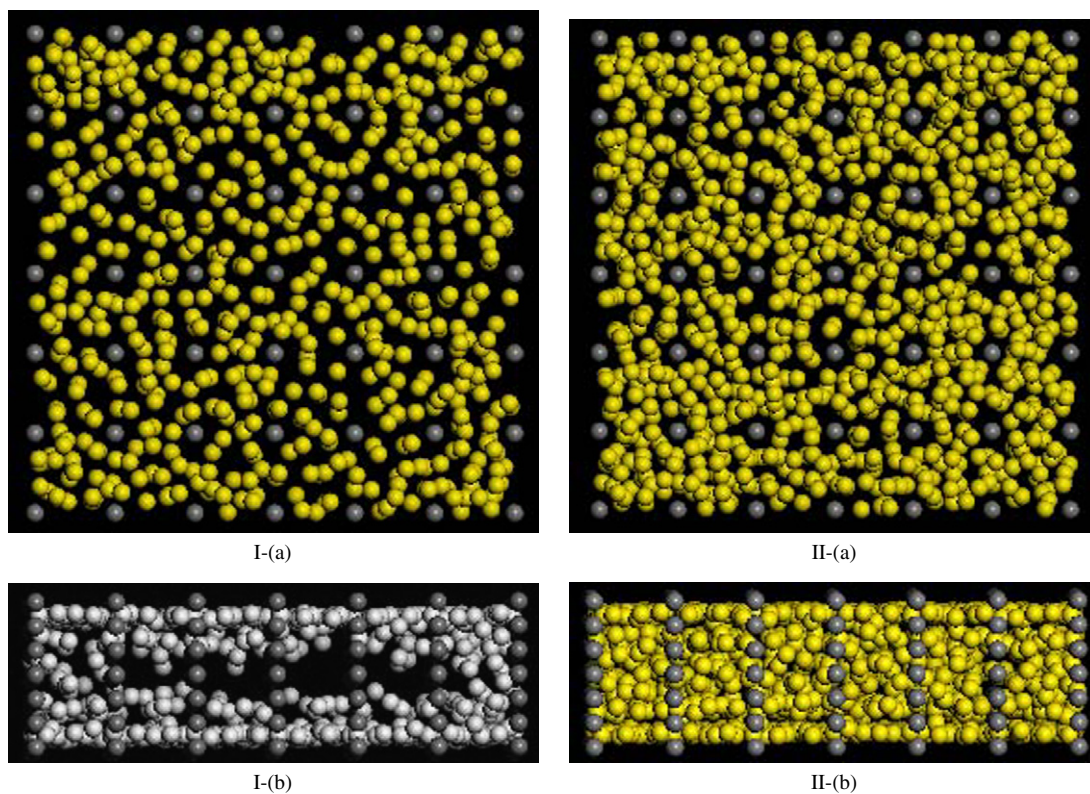


Fig. 6. Snapshots of carbon dioxide confined in pillared clays by the 1-site model at  $T = 228.15$  K,  $\psi = 0.94$ , and  $H = 2.38$  nm. (I)  $P/P_s = 0.47$ , (II)  $P/P_s = 0.68$ ; (a) from  $z$ -axis, (b) from  $y$ -axis.

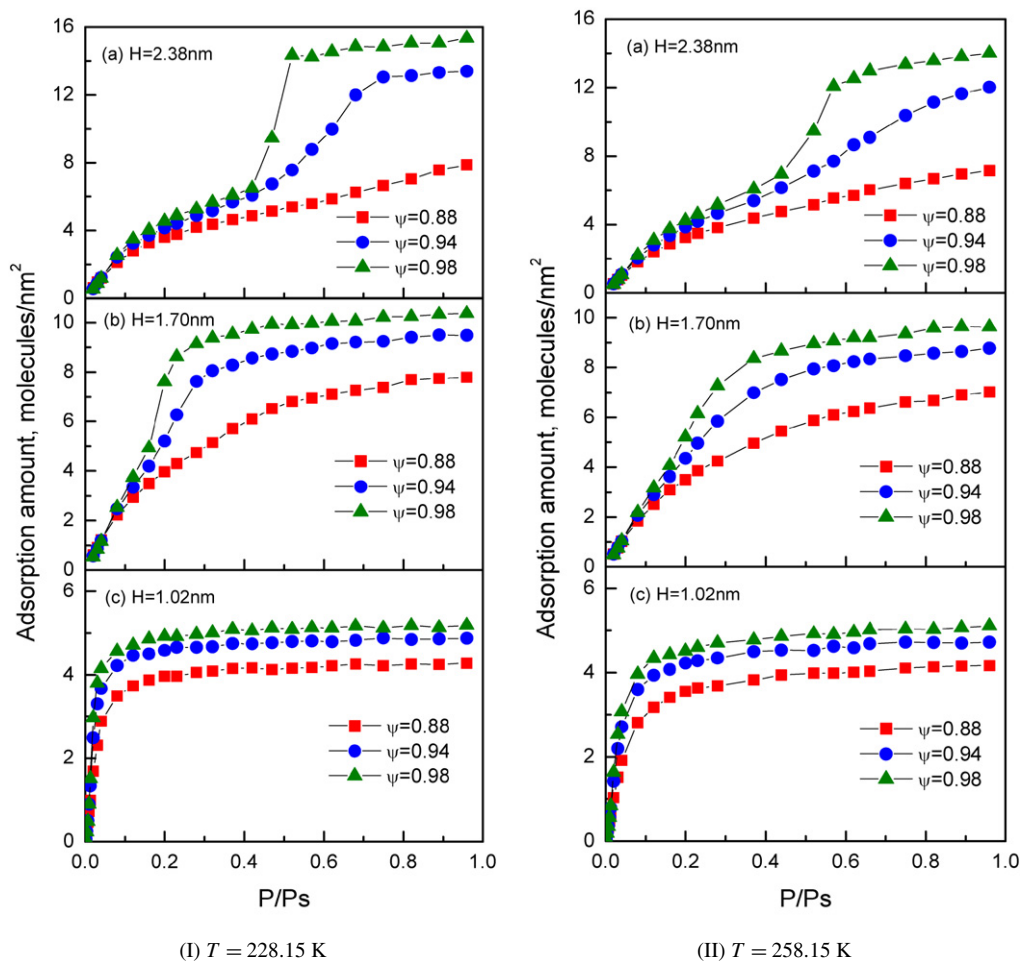


Fig. 7. Adsorption amounts of carbon dioxide changing with pressure at different porosities and pore widths and two subcritical temperatures: (I) 228.15 K ( $P_s = 0.84$  MPa), (II) 258.15 K ( $P_s = 2.29$  MPa); (a)  $H = 2.38$  nm, (b)  $H = 1.70$  nm, (c)  $H = 1.02$  nm.

a linear change at high temperature  $T = 258.15$  K (see Fig. 7, II-(a)). This difference can be explained in terms of the microscopic structure of the fluid confined in pores. The local density profiles of carbon dioxide at  $\psi = 0.94$ ,  $H = 2.38$  nm, and the two temperatures have been shown in Fig. 4, I-(a) and I-(b). Clearly, at  $P/P_s = 0.68$ , the local density presents multiple relatively pronounced peaks for the temperature of  $T = 228.15$  K, demonstrating that multiple adsorption layers appear in the pores. In contrast, only one inner layer arises at  $P/P_s = 0.47$ . The analysis of snapshots also convinces this phenomenon. As is indicated in Fig. 5, II, capillary condensation occurs at  $P/P_s = 0.68$ , corresponding to the first order jump in the adsorption isotherm. However, the saturated filling is not reached at  $P/P_s = 0.47$  yet, in spite of most of fluid molecules aggregating not only on the walls but also around the pillars in the pores (see Fig. 5, I). The behavior of  $T = 258.15$  K is similar to that of  $T = 228.15$  K at  $P/P_s = 0.44$ . However, the multiple inner layers give extremely slight peaks for  $P/P_s = 0.66$ , leading to just a simple linear increase of the isotherm for  $\psi = 0.94$ , rather than the S-shaped type at 228.15 K.

As seen in Fig. 7, the adsorption amount increases with pore width or porosity, and always exhibits the highest value at the largest  $H = 2.38$  nm or the greatest  $\psi = 0.98$  for the

two temperatures. In addition, there exists a visible transition of adsorption isotherm from type I to type IV with the increase of pore width from  $H = 1.02$  nm to  $H = 2.38$  nm. Nevertheless, this transition only takes place at the larger porosities of  $\psi = 0.94$  and  $0.98$ . It is noticed that at the narrowest pore width of  $H = 1.02$  nm, the isotherm shape is not inflected by the porosity  $\psi$ , and all present the isotherm of type I. However, at the larger pore of  $H = 1.70$  and  $H = 2.38$  nm, the porosity  $\psi$  alters the shape of the isotherms remarkably. For example, at  $T = 228.15$  K and  $H = 1.70$  and  $2.38$  nm, the adsorption isotherm increases almost linearly with pressure at  $\psi = 0.88$ , but shows a clear first order jump gradually with the ascending of  $\psi$  up to  $0.94$  and  $0.98$ . In short, our simulations demonstrate that not only temperature changes pronouncedly the shape of adsorption isotherms, but also pore width, especially porosity is a very important factor to affect the phase behavior of adsorption of fluid confined in pillared clays.

#### 4.3. Supercritical adsorption of carbon dioxide in pillared clays

In the past few years, the adsorption of supercritical fluids has attracted the interest of many researchers for understanding its special features in both experimental and theoretical fields.

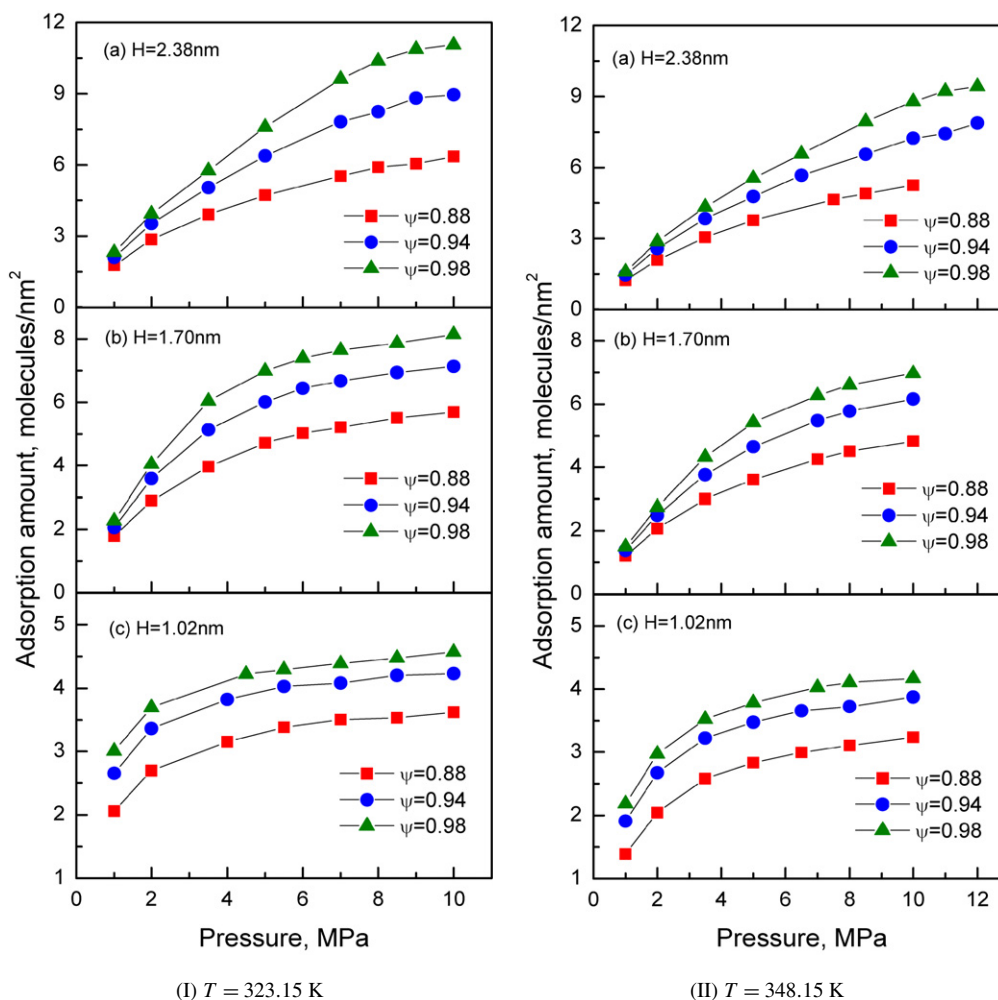


Fig. 8. Adsorption amounts of carbon dioxide versus pressure at different porosities and pore widths as well as two supercritical temperatures: (I) 323.15 K, (II) 348.15 K; (a)  $H = 2.38$  nm, (b)  $H = 1.70$  nm, (c)  $H = 1.02$  nm.

More significantly, carbon dioxide is widely used as a solvent in supercritical reaction processes for its mild critical condition, easy availability, nonflammability and nontoxicity [23]. Consequently, in this section, we will consider the supercritical adsorption of carbon dioxide in pillared clays. Fig. 8 shows the simulated adsorption isotherms at  $T = 323.15$  K and 348.15 K. The adsorption isotherm is very similar to each other at both temperatures, depicting a nearly linear increase with pressure for every pore width and porosity. In addition, the adsorption loading decreases with the increase of temperature at fixed pore width and porosity, and the adsorption amount at larger porosity is always higher than that at the smaller one.

The excess adsorption amount, also called Gibbs adsorption [34], is equal to the density in adsorption phase minus that in gas phase. Here, we use the excess amount per unit surface area to describe the excess adsorption. Fig. 9 presents the excess adsorption isotherms of carbon dioxide at different pore widths and porosities. As is expected, all figures indicate that the excess uptake exhibits a maximum, and then falls as pressure increases, which is in agreement with previous results [20, 35–37]. Furthermore, at the lower temperature  $T = 323.15$  K close to critical temperature  $T_c = 304.2$  K, an enhanced ad-

sorption and pronounced cuplike [35,38] maximum is observed for the larger pore width  $H = 2.38$  nm and porosity  $\psi = 0.98$ . It is noticeable that the excess uptake always gives the greater value at the larger porosity  $\psi = 0.98$ . In addition, no crossover is observed on their excess isotherms. Interestingly, the optimal pressure corresponding to the maximum is the same basically at the fixed pore width. That is to say, the porosity has no significant effect to the optimal pressure. However, the pore width presents a distinct effect on the optimal pressure. For the two temperature of  $T = 323.15$  and 348.15 K, the optimal pressure increases linearly with the pore width at  $\psi = 0.94$ .

## 5. Conclusions

We have investigated the adsorption behavior of carbon dioxide confined in pillared clays by constant pressure Gibbs ensemble Monte Carlo method. The calculated results at  $T = 228.15$  and 258.15 K demonstrate that the adsorption isotherms from the two models are consistent with each other basically. However, the local density presents a significant difference, because the shoulder in the main peak near the wall from the 3-site model can reflect the orientation of carbon dioxide, but

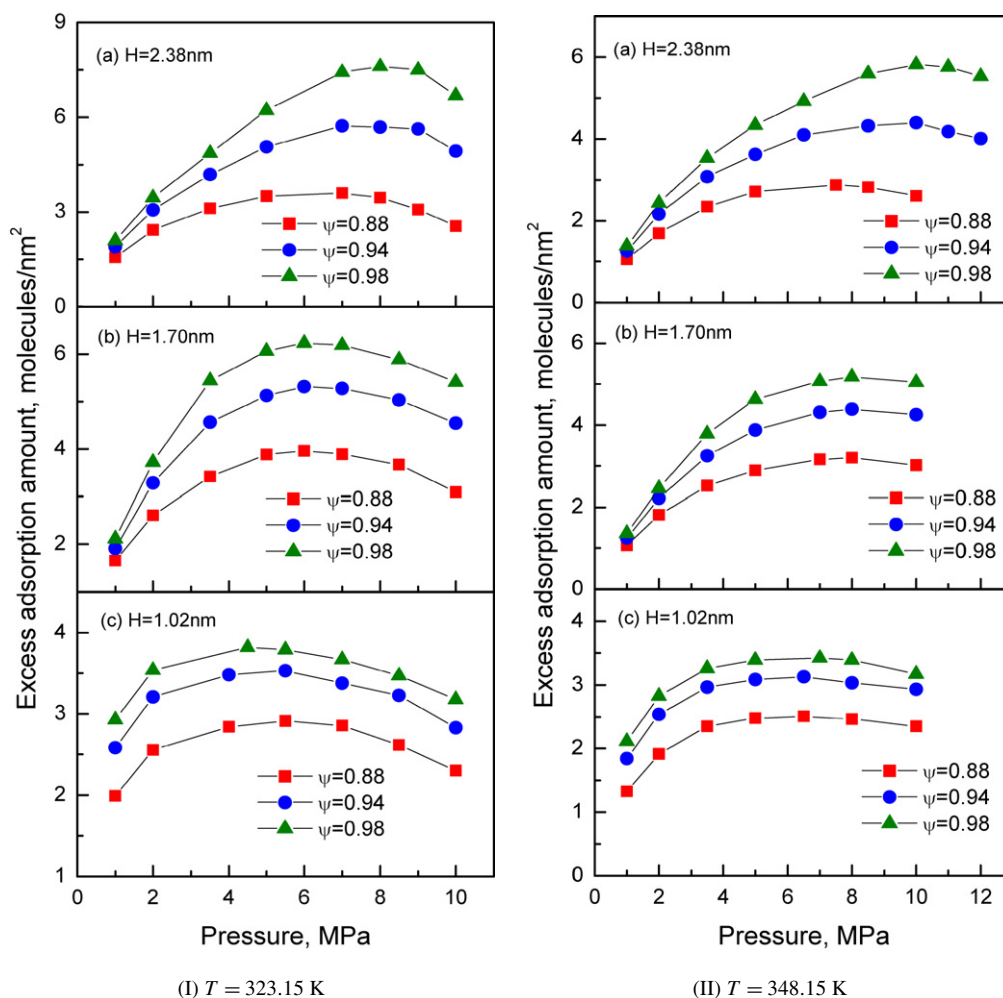


Fig. 9. Excess adsorption of carbon dioxide versus pressure at different porosities and pore widths as well as two supercritical temperatures: (I) 323.15 K, (II) 348.15 K; (a)  $H = 2.38$  nm, (b)  $H = 1.70$  nm, (c)  $H = 1.02$  nm.

no shoulder appears in the main peak for the 1-site model. Therefore, in the systematical investigations for exploring the effect of the porosity and the pore width on the adsorption of carbon dioxide in pillared clays, we used the 3-site model. It is observed that for the narrow pore of  $H = 1.02$  nm, each isotherm shape displays type I curve. Furthermore, the porosity did not affect the isotherm shape. However, for the larger pores of  $H = 1.70$  and  $H = 2.38$  nm, the increase of the porosity alters the shape of the adsorption isotherm from a simple linear relation to the first order jump, indicating that in this case the porosity plays a very important role on the isotherm shape and phase behavior of fluids confined in pillared clays. In addition, we also explored the excess adsorptions of carbon dioxide at supercritical temperature of  $T = 323.15$  and  $348.15$  K. It is observed that each excess isotherm appears a maximum, and the optimal pressure corresponding to the maximum increases with the pore width. However, the porosity has no significant effect on the optimal pressure.

It should be pointed out that the pillared clays model used here neglects many features of real porous materials [39], including the structural heterogeneity such as the presence of functional groups and impurities, and the surface heterogene-

ity arising from networking effects, crystallographic and surface irregularities. In addition, the adsorption of carbon dioxide with a quadrupolar moment would be definitely favored on polar adsorbents of pillared clays [40]. Nevertheless, we believe these results provide considerably useful information, at least partly, which can be applied to carbon dioxide recovery and natural gas purification to interpret the adsorption behavior from micro-scale molecular level. We expect more extensive studies of these neglected effects in our future work.

### Acknowledgments

This work is supported by the National Natural Science Foundation of China (Nos. 20646001, 20236010), the Program for New Century Excellent Talents in University (NCET), the National Basic Research Program (No. 203CB615807), and “Chemical Grid Project” and Excellent Talent Funding of Beijing University of Chemical Technology.

### References

- [1] H. Carola, Environ. Sci. Technol. A 32 (1) (1998) 20A–25A.
- [2] J.H. Howard, Environ. Sci. Technol. A 35 (7) (2001) 148A–153A.

- [3] V. Marry, P. Turq, *J. Phys. Chem. B* 107 (2003) 1832–1839.
- [4] X. Peng, W.C. Wang, R.S. Xue, Z.M. Shen, *AIChE J.* 52 (2006) 994–1003.
- [5] P. Cool, E.F. Vansant, *Sci. Technol.* 1 (1998) 265–288.
- [6] <http://www.uni-kiel.de/anorg/lagaly/ECGA/history.htm>.
- [7] F. Rouquerol, J. Rouquerol, K.S.W. Sing, *Adsorption by Powders and Porous Solids*, Academic Press, London, 1999, p. 373.
- [8] R.T. Yang, *Adsorbents: Fundamentals and Applications*, Wiley, New Jersey, 2003, p. 260.
- [9] R.A. Schoonheydt, T. Pinnavaia, G. Lagaly, N. Gangas, *Pure Appl. Chem.* 71 (12) (1999) 2367–2371.
- [10] A. Vaccari, *Appl. Clay Sci.* 14 (1999) 161–198.
- [11] M.S.A. Baksh, R.T. Yang, *AIChE J.* 38 (1992) 1357–1368.
- [12] A. Molinard, E.F. Vansant, *Adsorption* 1 (1995) 49–59.
- [13] P.R. Pereira, J. Pires, M.B.D. Carvalho, *Langmuir* 14 (1998) 4584–4588.
- [14] A. Gil, L.M. Ganda, *Chem. Eng. Sci.* 58 (2003) 3059–3075.
- [15] X.H. Yi, K.S. Shing, M. Sahimi, *AIChE J.* 41 (1995) 456–468.
- [16] X.H. Yi, J. Ghassemzadeh, K.S. Shing, M. Sahimi, *J. Chem. Phys.* 108 (1998) 2178–2188.
- [17] J. Ghassemzadeh, L.F. Xu, T.T. Tsotsis, M. Sahimi, *J. Phys. Chem. B* 104 (2000) 3892–3905.
- [18] D.P. Cao, W.C. Wang, *Phys. Chem. Chem. Phys.* 4 (2002) 3720–3726.
- [19] D.P. Cao, W.C. Wang, *Phys. Chem. Chem. Phys.* 3 (2001) 3150–3155.
- [20] D.P. Cao, W.C. Wang, X. Duan, *J. Colloid Interface Sci.* 254 (2002) 1–7.
- [21] Q.Y. Yang, X.P. Bu, C.L. Zhong, Y.G. Li, *AIChE J.* 51 (2005) 281–291.
- [22] X. Peng, W.C. Wang, S.P. Huang, *Fluid Phase Equilib.* 231 (2005) 138–149.
- [23] J. Zhou, W.C. Wang, *Langmuir* 16 (2000) 8063–8070.
- [24] M. Heuchel, G.M. Davies, E. Buss, N.A. Seaton, *Langmuir* 15 (1999) 8695–8705.
- [25] M.B. Sweatman, N. Quirke, *Langmuir* 17 (2001) 5011–5020.
- [26] J.G. Harris, K.H. Yung, *J. Phys. Chem.* 99 (1995) 12021–12024.
- [27] W.A. Steele, *Surf. Sci.* 36 (1973) 317–352.
- [28] S.C. McGrother, K.E. Gubbins, *Mol. Phys.* 97 (1999) 955–965.
- [29] A.Z. Panagiotopoulos, *Mol. Phys.* 62 (1987) 701–719.
- [30] D.P. Cao, J.Z. Wu, *Carbon* 43 (2005) 1364–1370.
- [31] A. Vishnyakov, P.I. Ravikovitch, A.V. Neimark, *Langmuir* 15 (1999) 8736–8742.
- [32] D.D. Do, H.D. Do, *Colloids Surf. A* 277 (2006) 239–248.
- [33] S. Brunauer, L.S. Demings, W.E. Deming, E. Teller, *J. Am. Chem. Soc.* 62 (1940) 1723–1732.
- [34] M. Sudibandriyo, Z. Pan, J.E. Fitzgerald, R.L. Robinson, A.M. Gasem, *Langmuir* 19 (2003) 5323–5331.
- [35] Z. Tan, K.E. Gubbins, *J. Phys. Chem.* 94 (1990) 6061–6069.
- [36] L. Zhou, Y.P. Zhou, M. Li, P. Chen, Y. Wang, *Langmuir* 16 (2000) 5955–5959.
- [37] O. Di Giovanni, W. Dorfler, M. Mazzotti, M. Morbidelli, *Langmuir* 17 (2001) 4316–4321.
- [38] P. Kowalczyk, H. Tanaka, K. Kaneko, A.P. Terzyk, D.D. Do, *Langmuir* 21 (2005) 5639–5646.
- [39] A. Gil, G. Yu, S.A. Korili, *J. Chem. Eng. Data* 49 (2004) 639–641.
- [40] P.R. Pereira, J. Pires, M. Brotas, *Langmuir* 14 (1998) 4584–4588.